ADVANCED OPTICAL MATERIALS
www.advopticalmat.de

Tailored Nonlinear Anisotropy in Mie-Resonant Dielectric Oligomers

*Maria K. Kroychuk, Damir F. Yagudin, Alexander S. Shorokhov, Daria A. Smirnova, Irina I. Volkovskaya, Maxim R. Shcherbakov, Gennady Shvets, Yuri S. Kivshar, and Andrey A. Fedyanin**

The field of Mie-resonant nanophotonics has attracted a lot of attention recently due to many promising applications in linear and nonlinear metaoptics. Optically induced magnetic resonances define novel characteristics of isolated high-index dielectric nanoparticles and their oligomers. Here, the orientation-dependent nonlinear frequency generation from dielectric oligomers with different symmetries, being all characterized by isotropic linear response, is demonstrated. The rotational dependence of the third-harmonic signal emitted by the nanoparticle oligomers in accord with their point-group symmetry (e.g., C3 or C4) is observed experimentally, while their linear scattering remains isotropic. The experimental data are in a good agreement with numerical simulations and the symmetry analysis of the nonlinear susceptibility tensor. The results open a new avenue for tailoring nonlinear properties of nanoscale structures.

1. Introduction

The study of Mie-resonant nanostructures based on high-index dielectric nanoparticles has emerged recently as a promising alternative for plasmonics.[1–3] Such nanoparticles are known to sustain both electric and magnetic dipolar and multipolar Mie-type resonances in the visible and near-IR spectral ranges,[4,5] and they can be used as building blocks for highly efficient metadevices and ultrathin metasurfaces.[6–9] Contrary to their plasmonic counterparts, all-dielectric nanoparticles do not suffer from nonradiative losses, and they allow novel functionalities. Owing to a strong local-field confinement in the volume of such nanostructures, as well as high stability under strong laser radiation, Mie-resonant nanoparticles are very attractive for nonlinear nanoscale photonics.[10–13] As an example, enhanced nonlinear optical harmonic generation has been predicted and demonstrated for a number of all-dielectric systems, ranging from single resonant nanoparticles[14–18] and nanoparticle arrays[19–21] to more special structures supporting subradiant anapole modes[22–25] and bound states in the continuum.[26]

When resonant nanoparticles are placed close to each other to form subwavelength clusters (also known as oligomers), novel effects such as the mode hybridization[27] and formation of electric and magnetic hot spots[28] emerge. These effects result from the near-field coupling between the constituent nanoparticles spawning an assortment of collective modes. The collective modes and their interference can result in pronounced asymmetric spectral features in the linear response of the nanoparticle oligomers, often associated with the Fano resonances.[29–34] Nonlinear response of oligomers and its link to the structure symmetry have been studied as well.[35–38] Although the study of nonlinear effects with isolated dielectric resonant nanoparticles received a considerable attention in nonlinear nanophotonics, their clusters and oligomers have not been utilized yet to tailor anisotropic properties of their nonlinear response.

In this paper, we study all-dielectric nanoparticle clusters composed of one, three, or four identical silicon nanodisks and reveal a strongly anisotropic nonlinear response, while their linear scattering remains isotropic. The pronounced orientation angle-dependence of the generated third-harmonic (TH) signal discloses the intrinsic symmetries of the nanoparticle oligomers, which are otherwise not accessible through the linear scattering data. We provide numerical simulations of the nonlinear response, which confirm the observed experimental signatures of the C3 and C4 point-group symmetries of the oligomers. Notably, the symmetry analysis of the effective nonlinear susceptibility tensors reveals that in the C3 case only out-of-plane nonlinear dipoles are responsible for the effective anisotropy. We believe these results can provide a viable path

M. K. Kroychuk, D. F. Yagudin, Dr. A. S. Shorokhov, Dr. M. R. Shcherbakov, Prof. A. A. Fedyanin
Faculty of Physics
Lomonosov Moscow State University
119991 Moscow, Russia
E-mail: fedyanin@nanolab.phys.msu.ru
Dr. D. A. Smirnova, Prof. Y. S. Kivshar
Nonlinear Physics Centre
Australian National University
Canberra, ACT 2601, Australia
Dr. D. A. Smirnova, I. I. Volkovskaya
Institute of Applied Physics
Nizhny Novgorod 603950, Russia
Dr. M. R. Shcherbakov, Prof. G. Shvets
School of Applied and Engineering Physics
Cornell University
Ithaca, NY 14853, USA
The ORCID identification number(s) for the author(s) of this article can be found under https://doi.org/10.1002/adom.201900447.

DOI: 10.1002/adom.201900447

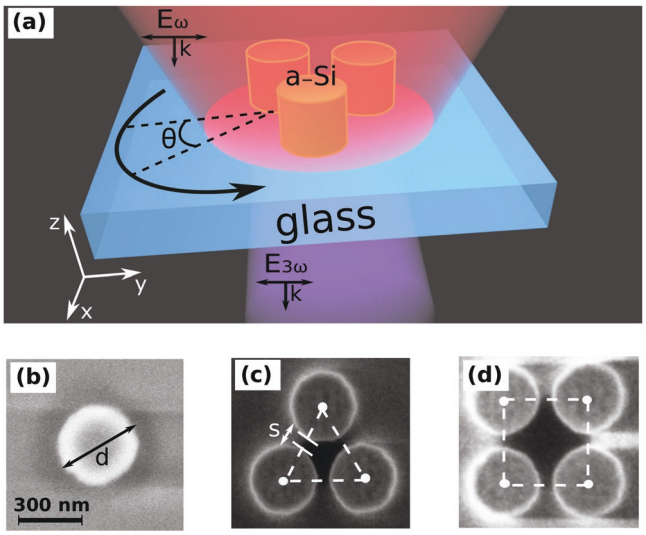

Figure 1. a) Schematic representation of the THG microscopy of isolated oligomers. TH intensity in transmission is measured as a function of the sample azimuthal rotation angle. b–d) Scanning electron microscope images of the nanoparticles under study. A monomer—an isolated silicon nanodisk (b); a trimer—three silicon nanodisks located at the vertices of an equilateral triangle (c); a quadrumer—four silicon nanodisks arranged in a square pattern (d).

toward artificially anisotropic nonlinear structures, expanding the scope of their applications in nonlinear nanoscale photonics.

2. Results and Discussion

The idea of the TH anisotropy characterization in all-dielectric oligomers is illustrated in **Figure 1**a. An axially symmetric isolated silicon nanoparticle in Figure 1b and nanoparticle oligomers—a trimer in Figure 1c and a quadrumer in Figure 1d—are illuminated by a normally incident infrared femtosecond laser beam. The TH signal emitted from the nanoparticles I_{TH} is measured for different sample orientation angles θ. Nonlinear anisotropy manifests itself as periodic features in $I_{TH}(\theta)$ that can be attributed to the presence of certain nonzero components in the effective nonlinear polarizability tensor $\hat{\chi}^{(3),\mathrm{eff}}$ that ties the TH polarization of the oligomer $\boldsymbol{P}^{(3)}(3\omega)$ and the pump field $\boldsymbol{E}(\omega):\boldsymbol{P}^{(3)}(3\omega)=\hat{\chi}^{(3),\mathrm{eff}}(3\omega=\omega+\omega+\omega)\vdots\boldsymbol{E}(\omega)\boldsymbol{E}(\omega)\boldsymbol{E}(\omega)$.

The goal of this work is to show that the specific point-group symmetry of the oligomer—C3 for the trimer and C4 for the quadrumer—can be used to tailor the symmetry of the nonlinear optical response, even though in the linear response there are no indications of such a symmetry.

A set of oligomer samples is made from a film of hydrogenated amorphous silicon with a thickness of 260 nm deposited on a fused silica substrate. Using the consequent processes of electron beam lithography and reactive ion etching, arrays of nanostructures with different dimensions were defined. The samples under study are isolated single nanodisks, monomers (Figure 1b), trimers formed by three silicon nanodisks located at the vertices of an equilateral triangle (Figure 1c), and quadrumers composed of four silicon nanodisks situated at the vertices of a square (Figure 1d). The spacing between the nanodisks in trimers and quadrumers is $s = 50$ nm and $s = 70$ nm, respectively. The dimensions of the structures are chosen in a way that their resonant behavior is tuned to the wavelength of our femtosecond pulse source. The fabrication procedure is given in details in Section S1 (Supporting Information).

For characterization of the fabricated samples, an experimental setup based on ytterbium solid-state femtosecond laser with a central wavelength of 1050 nm and a pulse duration of 150 fs was assembled. The laser radiation was used both as the pump for TH measurements, and as a pump for the supercontinuum radiation source used for linear transmittance spectroscopy of individual oligomers, as shown in **Figure 2**a. The nonlinear part, N-lin in Figure 2a, consisted of two sections: the main channel with the sample under study (S) and the reference channel with the unstructured amorphous silicon film of the same thickness as the sample. In both cases, the collimated TH beam was directed to the cathode of a photomultiplier tube assembly (PMT). The voltage output of the PMT was analyzed by a lock-in amplifier coupled to an optical chopper (CH) that modulates the pump signal at a frequency of 283 Hz. The detected signal was proved to be of TH origin by checking its cubic dependence on the pump power, see Figure S1a (Supporting Information).

For linear spectroscopy, Lin in Figure 2a, the laser beam was focused onto the facet of a single-mode nonlinear photonic crystal fiber, where the supercontinuum radiation with a spectral range from 900 to 1200 nm was generated. The main part of the linear setup coincided with the nonlinear one. Light that was transmitted through the sample was analyzed with a near-infrared spectrometer. The relative transmittance spectra of oligomers were evaluated by dividing the spectra from the structure by the spectra from the sample area where the a-Si layer was etched away. The supercontinuum radiation and the laser radiation were adjusted to be focused to the same area of the sample.

The result of the transmittance spectroscopy measurements for trimers and quadrumers with various nanodisk sizes is that there are pronounced resonance dips in the transmittance spectra at the carrier laser wavelength ($\lambda = 1050$ nm). Typical spectra of the two types of oligomers are presented in Figure 2b for a resonant trimer with $d = 285$ nm (blue dots) and a resonant quadrumer with $d = 270$ nm (red dots). The small vertical blue bar on the spectrum of the resonant trimer indicates the typical error of the transmittance data. In order to identify the origin of the dip, the spectrum of the resonant trimer with the parameters taken from its scanning electron microscopy (SEM) image ($d = 285$ nm, $s = 50$ nm) was calculated using Lumerical FDTD software (Figure 2c, red curve). The electric field distribution inside one of the nanodisks for the wavelength corresponding to the dip in the transmittance spectrum marks the excitation of the magnetic dipole (MD) Mie-type resonance in each nanoparticle. Strong light localization inside the nanostructure in the spectral vicinity of the Mie-type MD resonance was shown to dramatically enhance the nonlinear optical response of individual silicon nanoparticles.[13,16] The presence of the MD mode was essential for the choice of the oligomers for further linear and nonlinear experiments. The mismatch

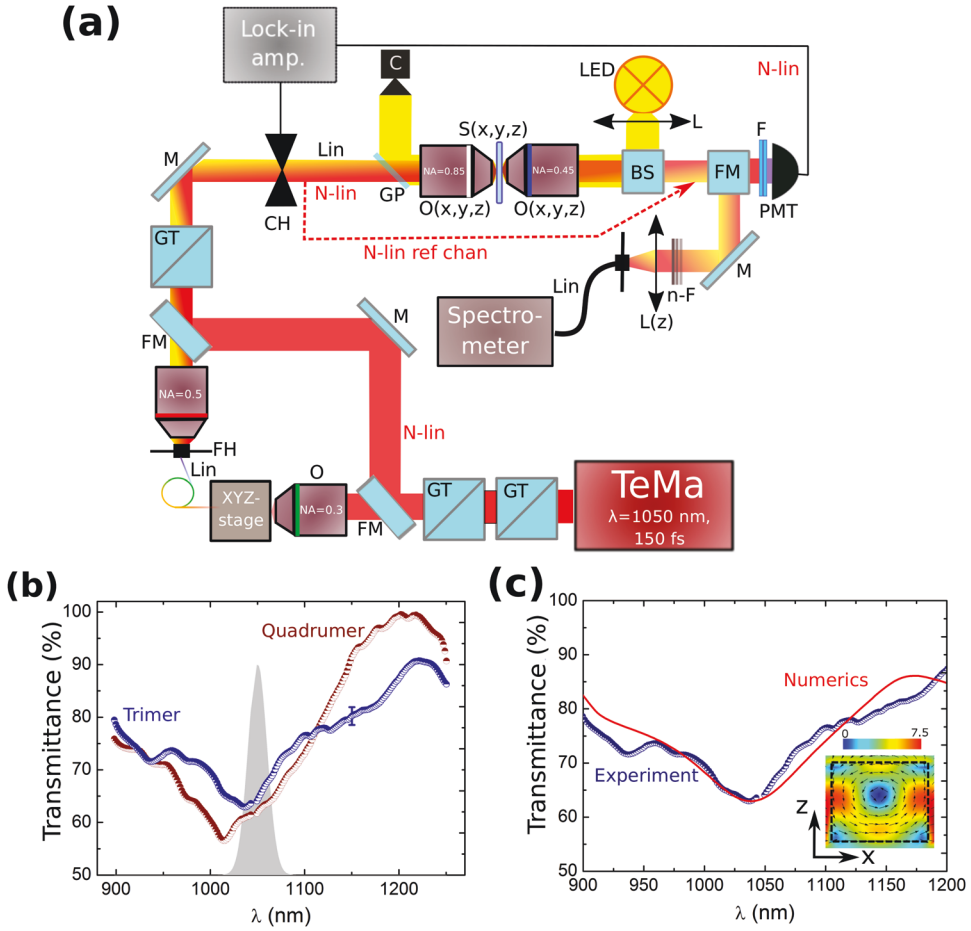

Figure 2. a) Schematic of the TH nonlinear microscopy setup (N-lin) and linear microscopy setup (Lin) based on an ytterbium solid-state femtosecond laser: GT are Glan-Taylor polarizers, BS is a beam splitter, FM is a mirror on a flipper mount, O are objective lenses mounted on micrometer stages, FH is a fiber holder, M is a metallic mirror, CH is an optical chopper, GP is a glass plate, C is a camera, S is the sample on a three-coordinate micrometer stage that allows azimuthal sample rotation, L are optical lenses, LED is a diode lamp, F is a set of BG39 filters, PMT is a photomultiplier assembly connected to a lock-in amplifier, n-F is a set of neutral density filters; the dashed red line illustrates the reference channel with an amorphous silicon film as a source of the reference TH output. b) Experimental transmittance spectra of the isolated trimer and quadrumer with various diameters (285 and 270 nm, respectively). c) Experimental (blue) and numerical (red) transmittance spectra of the isolated trimer with $d = 285$ nm and $s = 50$ nm. The inset to the right shows the electric field distribution inside one of the nanodisks at the central wavelength of the laser ($\lambda = 1050$ nm), which corresponds to the MD resonance of the single disk in the oligomer.

between experimental and numerical spectra in Figure 2 can be explained by the joint influence of experimental technique complexity, fabrication inaccuracy, and material dispersion deviations.

Figure 3a shows the transmittance of the trimers and quadrumers, described previously, excited at their MD resonance (1050 nm) for various source polarization azimuthal angles. The polarization rotation is carried out with a half-wave plate inserted after the optical chopper before the glass plate. For each azimuthal angle, the minimum of the transmitted power is obtained by scanning the sample position in its surface plane, ensuring the proper focusing at the oligomer. As predicted in Figure S2a,b (Supporting Information), the linear response of the oligomer is not affected by the pump polarization rotation within an error corridor of about 3%.

By using the scanning stage method to determine the optimum focusing conditions for each value of θ, as described in Section S2 (Supporting Information), we have measured the values of TH intensity from the samples as a function of θ, given with the red dots in Figure 3b–d. The results were, for each point, divided by the signal from the reference channel. Then we normalized obtained results to the maximum of each dependence. This normalization procedure allows elimination of the comparison of the absolute values of TH response and focusing only on its modulation. The $\theta = 0$ case corresponds to the electric field being parallel to a side of either the trimer or quadrumer. Figure 3b shows the TH signal generated from a single a-Si monomer pumped at its MD resonance (1050 nm). As expected, no appreciable oscillations in the TH intensity dependence on θ was observed. Figure 3c,d displays the measured $I_{TH}(\theta)$ from the trimer and quadrumer, respectively. The black curves show the Fourier transform of the experimental data with the main harmonics left in the decomposition; we justify our fitting strategy in the Discussion. For the trimer, the TH output oscillates with a period of $\pi/3$ rad, with the maximum relative modulation of the TH signal of ≈20%.

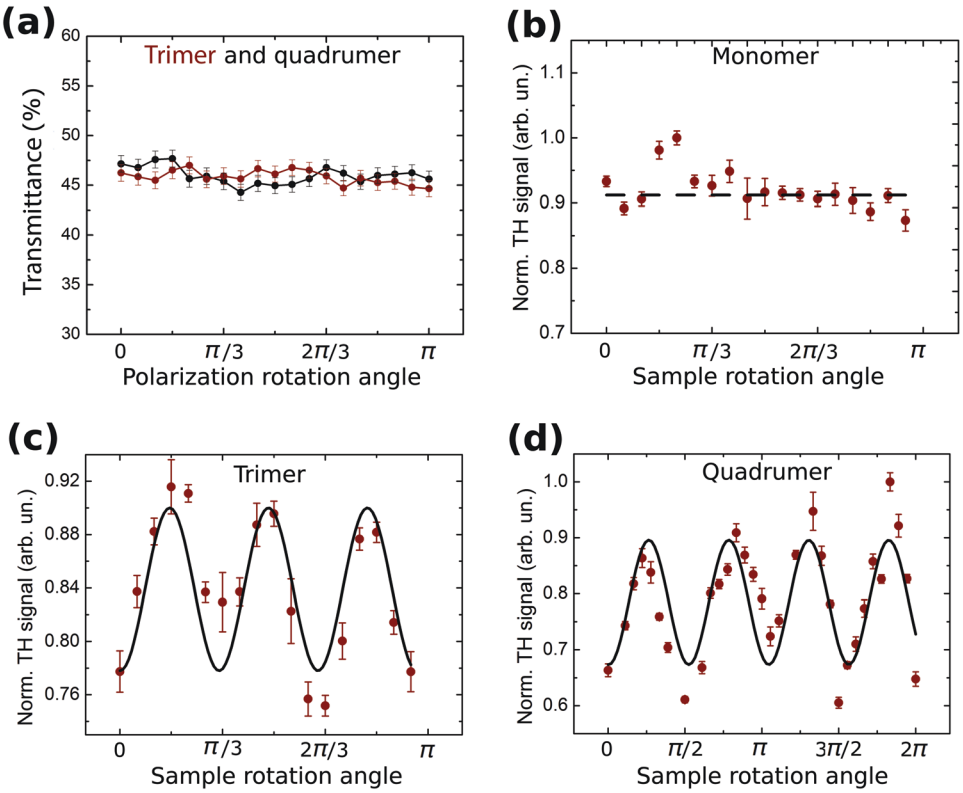

Figure 3. Experimental results. a) Transmittance of the trimer (s = 50 nm, d = 285 nm, red dots) and quadrumer (s = 70 nm, d = 270 nm, black dots) as a function of the polarization azimuthal angle for a fixed wavelength of λ = 1050 nm. b–d) TH microscopy of the isolated oligomers—TH intensity from the samples as a function of the azimuthal angle: monomer (b), trimer (c), and quadrumer (d). Solid black curves indicate sine approximations of the experimental results.

For the quadrumer, the oscillations in $I_{TH}(\theta)$ have a period of $\pi/2$ rad with almost 40% modulation. Far-field TH measurements are thereby able to reveal the underlying symmetry of the oligomer—distinguish trimer and quadrumer, in our case—which is not observed in their linear response (Figure 3a).

To support our experimental findings, we perform numerical modeling of the nonlinear electromagnetic response of the oligomers. **Figure 4**a shows the wavelength dependence of the scattering cross sections for the trimer and quadrumer. The spectra have similar resonant profiles: the maxima of the linear scattering for both oligomers are located near the fundamental wavelength of 1050 nm. The specific symmetry of oligomers is not distinguishable in the linear optical spectra. At the fixed pump wavelength, we then rotate the polarization of the incident plane wave to obtain the angular dependence of the total radiated TH power. The results of these simulations are summarized in Figure 4b–d. In accord with the experimental observations, the nonlinear response exhibits three peaks in the range [0; π] for the trimer and four peaks in the range [0; 2π] for the quadrumer, thus visualizing the characteristic rotational symmetry. The symmetry of TH response preserves the same tendency for the nonresonant oligomers (see Figure S3, Supporting Information), but the THG efficiency is significantly diminished because the MD mode of the nanostructure is no longer at the pump wavelength. When the spacing between the nanodisks in the oligomer is increasing, the local field coupling between them decreases and nanoparticles start to act as isolated objects. Thus, no appreciable oscillations in the TH intensity dependence on the θ were observed for the interparticle spacing of more than ≈285 nm (see Figure S4, Supporting Information).

At the fundamental wavelength, the clusters are subdiffractive, and the linear scattering is essentially determined by the total induced dipole moments of the cluster.[27] For the studied oligomers, the optical response is mostly governed by in-plane magnetic dipoles resonantly excited in each silicon disk. The nonlinear source inside each particle is driven by the magnetic resonance[10,39] and is roughly proportional to the magnetic dipole moment cubed $\propto|m_i^3(\omega)|$. The linear scattering for the rotationally symmetric oligomers does not depend on the polarization orientation (see Figure S2, Supporting Information, top row), as also supported by Hopkins et al.,[40] though the strength of MD excitations in particles changes upon rotation. At the TH frequency, the particles radiate as nonlinear antennas with the total emitted power being approximately the sum over particles, $P(3\omega) \propto \sum_i|m_i|^6$. These characteristic features are qualitatively reproduced in the framework of the coupled discrete dipole model, substituting the particles with effective electric and magnetic dipoles, as plotted in Figure S2 (Supporting Information). The implemented approach can be used for nonlinear diagnostics of subwavelength dielectric structures supporting multipolar optical

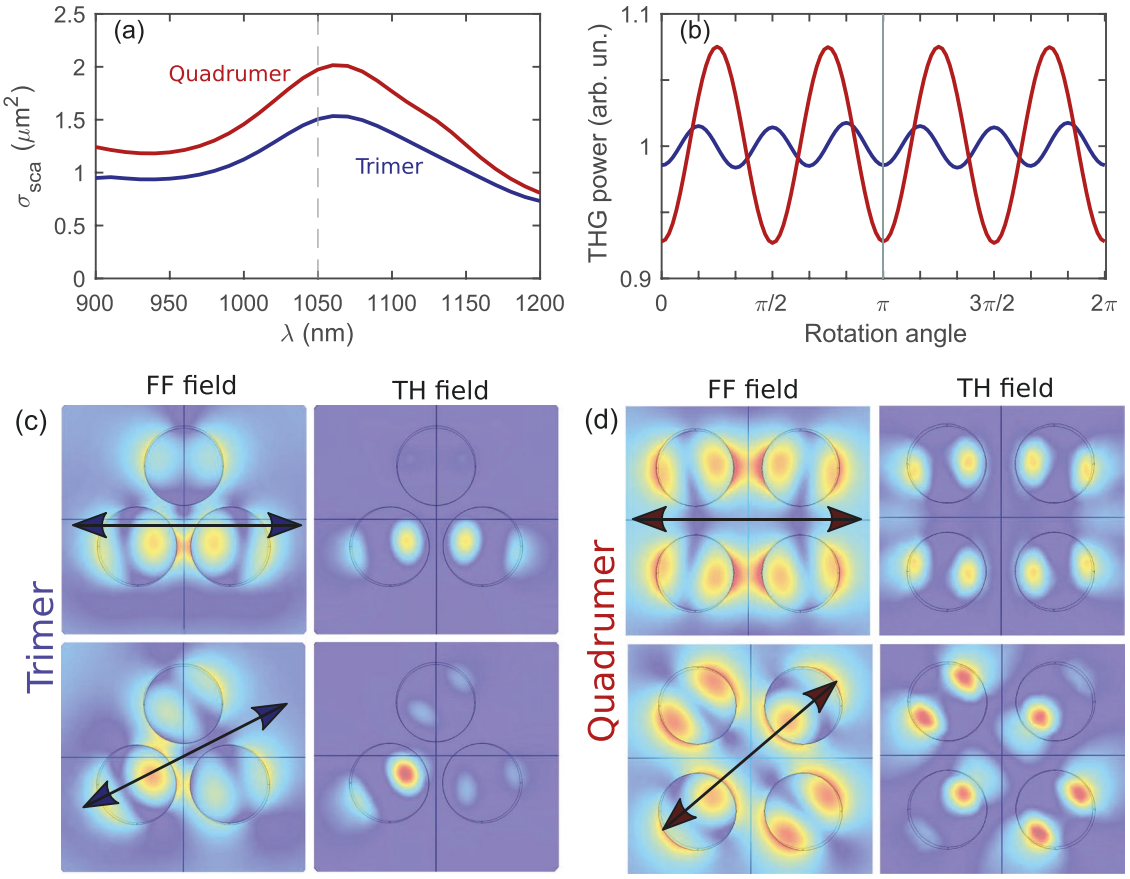

Figure 4. Numerical results. a) Scattering cross-section spectrum for the resonant oligomers of silicon nanodisks: trimer (blue) and quadrumer (red) at normal incidence. The dashed vertical gray line marks the laser wavelength position. b) TH power depending on the in-plane rotation angle of the pump polarization at fixed fundamental wavelength 1050 nm. The power is calculated over the full solid angle and independently normalized by the average power levels for each oligomer. c,d) Simulated near-field distributions at the fundamental and third-harmonic frequencies corresponding to the angles of minimum and maximum THG: c) [0, π/6] for trimer, and d) [0, π/4] for quadrumer. The false-color maps represent the absolute value of the electric field strength. The arrows indicate the electric field orientation in the incident wave.

resonances and hybrid systems, and it can be generalized to other nonlinear materials.

We additionally clarify the origin of the fitting curves in Figure 4 and the observed $I_{TH}(\theta)$ dependences with the effective model of the nonlinear response for the studied oligomers. The properties of the effective nonlinear susceptibility tensor $\hat{\chi}^{(3),\text{eff}}$ that can be assigned to the oligomer essentially reflects its structural symmetry.[41] In other words, the nonzero components of the tensor appear according to the symmetry of the oligomer, since amorphous silicon is isotropic and it does not contribute to anisotropy of the TH response. Exploiting the symmetry constraints, TH anisotropy functions $I_{TH}(\theta)$ can be calculated for arbitrary structures with C3 and C4 point group symmetries,[42] as described in Section S4 (Supporting Information). Given the expressions for the third-order nonlinear polarization $P_l^{(3)} \alpha \Sigma_{i,j,k} \chi_{lijk}^{(3),eff} E_i E_j E_k$, where $i, j, k, l = x, y, z$, the emitted TH intensity can be estimated as $I_{TH} \propto |P_x^{(3)}|^2 + |P_y^{(3)}|^2 + |P_z^{(3)}|^2$. Note that the latter expression is approximate, as it does not account for the optical response at the TH wavelength and the preferential detection direction that exists in the experimental setup. The TH output for C3-symmetric structures can be expressed as $I_{TH} \propto A - B\sin 6\theta$, where A and B are constants. It is peculiar to note that $B = \chi_{zxxx}^{(3),\text{eff}} = -\chi_{zxyy}^{(3),\text{eff}} = -\chi_{zyxy}^{(3),\text{eff}} = -\chi_{zyyx}^{(3),\text{eff}}$. This means that *only* nonlinear source induced perpendicular to the sample plane is responsible for the TH power alteration observed in Figure 3c, and the other components of $\hat{\chi}^{(3),\text{eff}}$ only account for the isotropic TH, as given by A. The resulting I_{TH} for the C3 symmetry contains three maxima and minima over the θ revolution from 0 to π, exactly as observed in the experiment. The third-order susceptibility tensor for a structure with the C4 symmetry leads to a more complicated TH intensity angular dependence, see Section S4 (Supporting Information), which, however, can be reduced to $I_{TH} \propto A - B\sin 4\theta$. This dependence shows four peaks over the full 2π revolution of θ, which agrees with the experiment. In contrast with the response of C3, for the C4 symmetry, components $P_x^{(3)}$ and $P_y^{(3)}$ are predominant, both for the isotropic response in A and the anisotropic response in B. This finding sheds light on the experimentally more shallow TH modulation for the trimer, in comparison with the quadrumer, in both experiment (Figures 3c,d) and calculations (Figure 4b). Such a pronounced difference in the nonlinear susceptibility tensor structure for objects that only differ in arrangement bears great promise for tailoring optical nonlinearities of nanoscale materials on demand.

3. Conclusion

In conclusion, we have predicted and observed experimentally the effective nonlinear anisotropy of symmetrically arranged resonant dielectric nanoparticle oligomers, induced by the near-field interaction between the nanoparticles. We have observed a strong dependence of the third-harmonic signal on the in-plane rotational angle in the nonlinear regime in accord with the intrinsic symmetry of oligomers, being not accessible through the linear scattering data. We have confirmed our experimental data by the numerical calculations of the effective anisotropic nonlinear response revealing the signatures of the C3 and C4 point-group symmetries in third-harmonic generation from the nanoparticle oligomers. The symmetry analysis of the effective nonlinear susceptibility tensors has demonstrated that in the C3 case only the out-of-plane nonlinear polarization is responsible for the anisotropic response. Our results provide a route toward novel nonlinear materials with engineered anisotropy based on Mie-resonant dielectric nanoparticles.

4. Experimental Section

Optical Characterization: Optical properties of the silicon nanodisk oligomer samples were examined using a setup for transmittance spectroscopy and THG microscopy (Figure 2a). Two adjacent Glan-Taylor prisms (GT) control the input laser beam power, the third GT prism controls the pump beam polarization. The mirror on the flipper mount (FM) separates the pump beam into two independent channels: the TH microscopy channel (N-lin) and the transmittance spectroscopy channel (Lin). N-lin channel itself is divided into the main part and reference part (N-lin ref chan). In the main channel, the horizontally polarized pump beam is focused by the objective lens with a numerical aperture NA = 0.85 to the spot with a waist diameter of ≈2.5 μm and a peak intensity up to 5 GW cm^{-2} in the sample plane. The sample is mounted on a motorized stage with a step size of ≈50 nm. The forward-propagating TH radiation is collected by an objective lens with a numerical aperture NA = 0.45 and is spectrally filtered out from the pump beam by a set of *BG*39 filters (F). The sample can be continuously rotated by the full angle $\theta = 2\pi$ in its plane. For switching between the reference and the main channels, a metallic mirror (M) is mechanically introduced. The reference channel consists of an aspheric lens (L), which focuses the pump beam onto the unstructured amorphous silicon film. The diode lamp (LED) combined with the lens (Figure 2a) was used to visualize an isolated nanodisk oligomer with the CMOS camera (C) in both linear and nonlinear schemes. After the lens (L) the radiation is focused by the objective lens on the sample, and then collected by the objective lens with NA = 0.85 and directed to the CMOS camera (C). Using the sample image on the camera, separate nanodisks of isolated oligomer structures can be recognized. The pump position is also independently indicated on the camera. The position of the sample can be scanned by a piezo-stage with the position accuracy of 50 nm. The detailed description of the setup and TH microscopy methods is given in Section S2 (Supporting Information).

Numerical Modeling: The optical response of the sample is calculated by using the finite-difference time-domain method in the Lumerical FDTD Solutions software. The nonlinear response of silicon nanodisks was modeled numerically with the use of FEM solver of COMSOL Multiphysics in frequency domain, with the method described in refs. [36] and [39]. The detailed information about numerical simulation is presented in Section S4 (Supporting Information).

Supporting Information

Supporting Information is available from the Wiley Online Library or from the author.

Acknowledgements

This work was performed in part at the Cornell NanoScale Facility, a member of the National Nanotechnology Coordinated Infrastructure (NNCI), which was supported by the National Science Foundation (Grant ECCS-1542081). Y.S.K. acknowledges the support from the Strategic Fund of the Australian National University. The work was performed under financial support of the Russian Ministry of Education and Science (Grant No. 14.W03.31.0008, development of the nonlinear microscopy setup), MSU Quantum Technology Center (FDTD calculations), and the Russian Science Foundation (18-12-00475 third-harmonic microscopy experiments and 15-02-00065 linear optical characterization). D.A.S. and I.I.V. acknowledge financial support by the Russian Foundation for Basic Research (Grants No. 18-02-00381, 19-02-00261). G.S. and M.R.S. acknowledge support by the Cornell Center for Materials Research with funding from the NSF MRSEC program (DMR-1719875). The authors are grateful to S. Dagesyan for the help with the SEM characterization.

Conflict of Interest

The authors declare no conflict of interest.

Keywords

all-dielectric nanoparticles, nonlinear anisotropy, third-harmonic microscopy

Received: March 13, 2019
Revised: June 3, 2019
Published online: July 28, 2019

[1] A. I. Kuznetsov, A. E. Miroshnichenko, M. L. Brongersma, Y. S. Kivshar, B. Luk'yanchuk, *Science* **2016**, *354*, aag2472.
[2] S. Kruk, Y. Kivshar, *ACS Photonics* **2017**, *4*, 2638.
[3] Y. Kivshar, *Natl. Sci. Rev.* **2018**, *5*, 144.
[4] A. I. Kuznetsov, A. E. Miroshnichenko, Y. H. Fu, J. Zhang, B. Luk'yanchuk, *Sci. Rep.* **2012**, *2*, 492.
[5] A. B. Evlyukhin, S. M. Novikov, U. Zywietz, R. L. Eriksen, C. Reinhardt, S. I. Bozhevolnyi, B. N. Chichkov, *Nano Lett.* **2012**, *12*, 3749.
[6] S. Kruk, B. Hopkins, I. I. Kravchenko, A. Miroshnichenko, D. N. Neshev, Y. S. Kivshar, *APL Photonics* **2016**, *1*, 030801.
[7] M. Decker, I. Staude, *J. Opt.* **2016**, *18*, 103001.
[8] P. Genevet, F. Capasso, F. Aieta, M. Khorasaninejad, R. Devlin, *Optica* **2017**, *4*, 139.
[9] L. Wang, S. Kruk, K. Koshelev, I. I. Kravchenko, B. Luther-Davies, Y. S. Kivshar, *Nano Lett.* **2018**, *18*, 3978.
[10] D. Smirnova, Y. S. Kivshar, *Optica* **2016**, *3*, 1241.
[11] A. Krasnok, M. Tymchenko, A. Alù, *Mater. Today* **2018**, *21*, 8.
[12] S. Liu, P. P. Vabishchevich, A. Vaskin, J. L. Reno, G. A. Keeler, M. B. Sinclair, I. Staude, I. Brener, *Nat. Commun.* **2018**, *9*, 2507.
[13] G. Della Valle, B. Hopkins, L. Ganzer, T. Stoll, M. Rahmani, S. Longhi, Y. S. Kivshar, C. De Angelis, D. N. Neshev, G. Cerullo, *ACS Photonics* **2017**, *4*, 2129.

[14] M. R. Shcherbakov, D. N. Neshev, B. Hopkins, A. S. Shorokhov, I. Staude, E. V. Melik-Gaykazyan, M. Decker, A. A. Ezhov, A. E. Miroshnichenko, I. Brener, A. Fedyanin, Y. Kivshar, *Nano Lett.* **2014**, *14*, 6488.
[15] L. Carletti, A. Locatelli, O. Stepanenko, G. Leo, C. De Angelis, *Opt. Express* **2015**, *23*, 26544.
[16] S. S. Kruk, R. Camacho-Morales, L. Xu, M. Rahmani, D. A. Smirnova, L. Wang, H. H. Tan, C. Jagadish, D. N. Neshev, Y. S. Kivshar, *Nano Lett.* **2017**, *17*, 3914.
[17] E. V. Melik-Gaykazyan, M. R. Shcherbakov, A. S. Shorokhov, I. Staude, I. Brener, D. N. Neshev, Y. S. Kivshar, A. A. Fedyanin, *Philos. Trans. R. Soc., A* **2017**, *375*, 20160281.
[18] G. Grinblat, Y. Li, M. P. Nielsen, R. F. Oulton, S. A. Maier, *ACS Photonics* **2017**, *4*, 2144.
[19] S. Kruk, A. Poddubny, D. Smirnova, L. Wang, A. Slobozhanyuk, A. Shorokhov, I. Kravchenko, B. Luther-Davies, Y. Kivshar, *Nat. Nanotechnol.* **2019**, *14*, 126.
[20] S. Liu, M. B. Sinclair, S. Saravi, G. A. Keeler, Y. Yang, J. Reno, G. M. Peake, F. Setzpfandt, I. Staude, T. Pertsch, I. Brener, *Nano Lett.* **2016**, *16*, 5426.
[21] P. P. Vabishchevich, S. Liu, M. B. Sinclair, G. A. Keeler, G. M. Peake, I. Brener, *ACS Photonics* **2018**, *5*, 1685.
[22] G. Grinblat, Y. Li, M. P. Nielsen, R. F. Oulton, S. A. Maier, *Nano Lett.* **2016**, *16*, 4635.
[23] T. Shibanuma, G. Grinblat, P. Albella, S. A. Maier, *Nano Lett.* **2017**, *17*, 2647.
[24] V. F. Gili, L. Ghirardini, D. Rocco, G. Marino, I. Favero, I. Roland, G. Pellegrini, L. Duò, M. Finazzi, L. Carletti, A. Locatelli, A. Lemaitre, D. Neshev, C. De Angelis, G. Leo, M. Celebrano, *Beilstein J. Nanotechnol.* **2018**, *9*, 2306.
[25] K. Baryshnikova, D. Smirnova, B. Lukýanchuk, Y. Kivshar, *Adv. Opt. Mater.* **2019**, *7*, 1801350.
[26] L. Carletti, K. Koshelev, C. De Angelis, Y. Kivshar, *Phys. Rev. Lett.* **2018**, *121*, 033903.
[27] B. Hopkins, A. N. Poddubny, A. E. Miroshnichenko, Y. S. Kivshar, *Phys. Rev. A* **2013**, *88*, 053819.
[28] R. M. Bakker, D. Permyakov, Y. F. Yu, D. Markovich, R. Paniagua-Domínguez, L. Gonzaga, A. Samusev, Y. Kivshar, B. Luk'yanchuk, A. I. Kuznetsov, *Nano Lett.* **2015**, *15*, 2137.
[29] B. Luk'yanchuk, N. I. Zheludev, S. A. Maier, N. J. Halas, P. Nordlander, H. Giessen, C. T. Chong, *Nat. Mater.* **2010**, *9*, 707.
[30] S. Zhang, K. Bao, N. J. Halas, H. Xu, P. Nordlander, *Nano Lett.* **2011**, *11*, 1657.
[31] C. Wu, A. B. Khanikaev, R. Adato, N. Arju, A. A. Yanik, H. Altug, G. Shvets, *Nat. Mater.* **2012**, *11*, 69.
[32] P. Fan, Z. Yu, S. Fan, M. L. Brongersma, *Nat. Mater.* **2014**, *13*, 471.
[33] K. E. Chong, B. Hopkins, I. Staude, A. E. Miroshnichenko, J. Dominguez, M. Decker, D. N. Neshev, I. Brener, Y. S. Kivshar, *Small* **2014**, *10*, 1985.
[34] M. Limonov, M. Rybin, A. Poddubny, Y. Kivshar, *Nat. Photonics* **2017**, *11*, 543.
[35] M. R. Shcherbakov, A. S. Shorokhov, D. N. Neshev, B. Hopkins, I. Staude, E. V. Melik-Gaykazyan, A. A. Ezhov, A. E. Miroshnichenko, I. Brener, A. A. Fedyanin, Y. Kivshar, *ACS Photonics* **2015**, *2*, 578.
[36] A. S. Shorokhov, E. V. Melik-Gaykazyan, D. A. Smirnova, B. Hopkins, K. E. Chong, D.-Y. Choi, M. R. Shcherbakov, A. E. Miroshnichenko, D. N. Neshev, A. A. Fedyanin, Y. S. Kivshar, *Nano Lett.* **2016**, *16*, 4857.
[37] M. Rahmani, A. S. Shorokhov, B. Hopkins, A. E. Miroshnichenko, M. R. Shcherbakov, R. Camacho-Morales, A. A. Fedyanin, D. N. Neshev, Y. S. Kivshar, *ACS Photonics* **2017**, *4*, 454.
[38] G. Bautista, C. Dreser, X. Zang, D. P. Kern, M. Kauranen, M. Fleischer, *Nano Lett.* **2018**, *18*, 2571.
[39] D. A. Smirnova, A. B. Khanikaev, L. A. Smirnov, Y. S. Kivshar, *ACS Photonics* **2016**, *3*, 1468.
[40] B. Hopkins, W. Liu, A. Miroshnichenko, Y. Kivshar, *Nanoscale* **2013**, *5*, 6395.
[41] Y.-R. Shen, *The Principles of Nonlinear Optics*, Wiley, New York **1984**.
[42] R. W. Boyd, *Nonlinear Optics*, Elsevier, Amsterdam **2003**.

